Behaviour of Silica during Metal Recovery from Bauxite Residue by Acidic Leaching

Rodolfo Marin Rivera[1], Brecht Ulenaers[2], Ghania Ounoughene[3], Koen Binnemans[4] and Tom Van Gerven[5]

1. PhD candidate
2. Student of M.Sc. Chemical Engineering
3. Research Associate
5. Professor

KU Leuven, Department of Chemical Engineering, Heverlee, Belgium

4. Professor

KU Leuven, Department of Chemistry, Heverlee, Belgium

Corresponding author: rodolfoandres.marinrivera@kuleuven.be

Abstract

Bauxite residue represents an interesting source for not only major elements such as aluminium, iron and titanium, but also for rare earths (REEs), while the residue after metal recovery can be used for low-carbon building materials and cementitious binders. Several methods based on direct acidic leaching for recovering metals from bauxite residue have been reported. The co-dissolution of iron represents a significant drawback for REEs recovery upon silica polymerization. The behaviour of silica has been studied during acidic leaching with concentrated mineral acid (H_2SO_4). The extraction of aluminium, iron and titanium is limited due to an insufficient amount of acidic solution for leaching caused by the polymerization of silica. Kinetic studies have demonstrated that at constant temperatures, silica dissolution increases with increasing acid concentration, but it decreases when the temperature is increased and the acid concentration is reduced. This is due to an enhancement in the solubility of monomeric silicic acid formed during acidic leaching. The control mechanisms of silica dissolution have been described according to the shrinking core model by a chemical reaction stage, i.e. silica polymerization, followed by a diffusion stage, because of the silica gel adsorbed on the surface of the particles that limits the metal extraction.

Key words: Dry digestion; silica; silicate; bauxite residue; red mud; rare earths.

1 Introduction

Bauxite residue (BR, also called red mud) represents an interesting source for major elements such as aluminium, iron and titanium, but also for rare-earth elements (REEs) [1]. Several methods based on direct leaching by acids have been reported for recovering valuable metals from bauxite residue [2–5]. The extraction efficiencies depend on the acid concentration with more extraction achieved at higher acid concentrations. Sulfuric acid leaching is considered to be the most versatile approach. However, higher acid concentrations also lower the silica solubility, which leads to a greater silicon supersaturation index (SSI). The SSI represents the ratio of dissolved silica with respect to the maximum silica solubility [6]. The increase of SSI is considered as the driving force for silica polymerization, also known as silica gel formation [7,8]. The formation mechanism of silica gel precipitation has been described in detail elsewhere [8–11].

Silica gel precipitation represents a serious drawback in the recovery of metals from ores and process residues by hydrometallurgical methods because the gel containing solutions can no

longer be filtered [12–14]. Additionally, this gelatinous precipitate may blind ore particles and reduce the leaching kinetics significantly.

Among others, quartz, sodalite and cancrinite are the most abundant silica bearing minerals in bauxite residue. Under standard conditions (1 atm, 25 °C), the solubility of quartz is about 6 mg L^{-1} whereas amorphous silica reaches a solubility of 100-120 mg L^{-1} under the same conditions. From this point of view, the contribution of soluble silica by quartz is negligible. The objective of this paper is to study the behavior of amorphous silica during leaching of bauxite residue with diluted H_2SO_4. Kinetic studies are performed at different concentrations and temperatures.

2 Material and Methods

The bauxite residue studied in this paper was kindly provided by Aluminium of Greece (Agios Nikolaos, Greece). It originates from a mixture of karst and lateritic bauxites. It was received from the alumina refinery after dewatering by filter pressing and drying at room temperature. Upon arrival in the lab, the sample was further dried at 105 ºC for 24 h. Chemical analysis of the major elements in bauxite residue was performed by wavelength dispersive X-ray fluorescence spectroscopy (WDXRF, Panalytical PW2400). The mineralogy of the samples was studied by X-ray powder diffraction (XRD, Bruker D2 Phaser). The obtained data were evaluated with EVA V.3.1 (Bruker AXS) and quantified with Topas-Academic V.5, using the Rietveld method.

Kinetics experiments were performed in a 150 mL glass reactor with H_2SO_4 (95-97 vol%, Sigma-Aldrich) solution of a fixed concentration (0.5 and 1.5 N). The experimental set-up consists of a hot-plate magnetic-stirrer device, a pH-electrode (Hamilton, VWR) and a thermocouple (Pt100, VWR). Within the reactor solid particles were mixed with 100 mL of the corresponding solution at a liquid-to-solid ratio (*L/S*) of 5:1. The entire experiment lasted for 60 min, in which aliquots of slurry were extracted from the glass reactor at specific time intervals. The mixtures were continuously agitated during the whole experiment in order to ensure a homogenous suspension. Each aliquot was filtered using a syringe and a 0.45 µm filter (CHROMAFIL PET-45/25 Polyester), and diluted with 2 vol% HNO_3 for Inductively Coupled Plasma Optical Emission Spectroscopy (ICP-OES, PerkinElmer Optima 8300) analysis for aluminium, iron, titanium and silicon. The experiments were conducted at different temperatures (25, 40, 60 and 80 °C). At the end of each experiment, the remaining reactor content was filtrated through a Buchner filter (VWR® Grade 413 Filter Paper, Qualitative, 5 µm retention), and the solid filter cake was dried (24 h, 105 °C) and stored for further XRD analysis.

3 Results and Discussion

3.1. Characterization of the Bauxite Residue

The chemical analysis of the major elements present in bauxite residue is shown in Table 1. Bauxite residue is rich in iron oxide and alumina. Mineralogical analysis allowed the identification of several mineral phases (Table 2), rich in iron (hematite, goethite), aluminium (gibbsite, diaspore, bayerite), calcium (calcite, calcium silicates and calcium aluminosilicates), sodium (sodalite, cancrinite) and titanium (rutile).

Table 1. Major chemical components, expressed as oxide, in the bauxite residue.

Metal as oxides	Concentration, wt%
Fe_2O_3	46.7
Al_2O_3	18.1
CaO	8.5
SiO_2	7.3
TiO_2	5.8
Na_2O	2.8
Loss on ignition	8.5

Table 2. Mineralogical composition of the bauxite residue sample (estimated relative error 10%).

Phase	Chemical composition	Concentration, wt%
Hematite	Fe_2O_3	36
Grossular	$Ca_3Al_2(SiO_4)_3$	13
Dicalcium-silicate (C2S)	Ca_2SiO_4	12
Gibbsite	$Al(OH)_3$	8
Diaspore	AlO(OH)	7
Tricalcium-silicate (C3S)	Ca_3SiO_5	5
Goethite	FeO(OH)	5
Calcite	$CaCO_3$	4
Bayerite	α-$Al(OH)_3$	4
Sodalite	$Na_6(Al_6Si_6O_{24})\cdot x NaOH\cdot(8-2x)H_2O$	3
Calcium-aluminium-silicate (CAS)	$Al_{12}CaO_{27}Si_4$	2
Rutile	TiO_2	2
Cancrinite	$Na_6Ca_2Al_6Si_6O_{24}(CO_3)_2\cdot 2H_2O$	1

3.2. Silicon Dissolution Behavior

Kinetic studies were conducted to identify the leaching behavior of silicon in the leachate. The experiments were conducted with H_2SO_4. Figure 1 describes the effect of H_2SO_4 on the dissolution of silicon (relative to the initial silicon content) as a function of time at different concentrations and temperature. At constant temperature, the dissolution of silicon (Si) in the leach solution increases with increasing acid concentration, and the maximum dissolution was obtained at 80 °C with 1.5 N H_2SO_4 after 1 hour of experiment. In sulfuric media, silicates dissolve from the bauxite residue by forming orthosilicic acid, H_4SiO_4, according to Equation 1. At relatively low pH values, i.e. below the isoelectric point for silica in the solution (pH_{iso} between 1.7 and 2.2) [10], the hydrolysis of silica occurs very fast to produce H_4SiO_4 and $H_3SiO_4^-$ (Equation 1 and 2), which are the precursors for silica gel polymerization [8,15]. Initially, silica monomers (e.g., H_4SiO_4, $H_3SiO_4^-$) polymerize via dimers, trimers, etc. to cyclic oligomers ($Si_{n+1}O_{m+2}\cdot OH$), according to Equations 3 and 4. These oligomers continue to react until a gel network is formed via Ostwald ripening, i.e. dissolution of smaller particles and precipitation on larger particles, which finally results in the formation of an acidic silica gel [7].

$$M_2SiO_{4(s)} + 2H_2SO_{4(l)} + H_2O_{(l)} \rightarrow 2MSO_{4(aq)} + H_2O_{(l)} + H_4SiO_{4\,(aq)} \quad (1)$$

$$H_4SiO_{4\,(aq)} + H_2O \rightarrow H_3SiO_4^- + H_3O^+ \quad (2)$$

$$H_3SiO_4^- + H_4SiO_4 \rightarrow OH^- + H_6Si_2O_7 \quad (3)$$

$$Si_nO_mOH + H_4SiO_4 \rightarrow Si_{n+1}O_{m+2}OH + 2H_2O \quad (4)$$

At low acid concentration, i.e. 0.5 N H_2SO_4, the dissolution rates in the first 3 – 4 minutes of chemical reaction are identical at different temperatures, but it decreases after that period of time when the temperature increases. This is due to the reduction of the monomer's solubility as consequence of a fast reactivity of the acid with solid particles [10]. Furthermore, the silica saturation index (SSI: dissolved silica concentration/silica solubility) increases when the temperature is increased due to an increase of monomeric silicic acid's solubility [10,16]. Therefore, the higher the temperature, the greater the rate of silica-gel formation. However, an increase in silicon dissolution at concentration of 1.5 N of H_2SO_4 was observed, particularly at high temperatures. This suggests that silicate compounds, such as grossular, C2S and C3S (Figure 2), are highly soluble in H_2SO_4. The low concentration of these compounds in the leached samples indicates a favoured dissolution of these compounds in H_2SO_4, which is enhanced by increasing the acid concentration. The initial concentration of silicon in the solution was about 3.9 g L^{-1} when the bauxite residue started being leached with 1.5 N of H_2SO_4, i.e. within the first 3 – 4 minutes, which represents the minimal concentration of silicon in the leachate for silica gel formation.

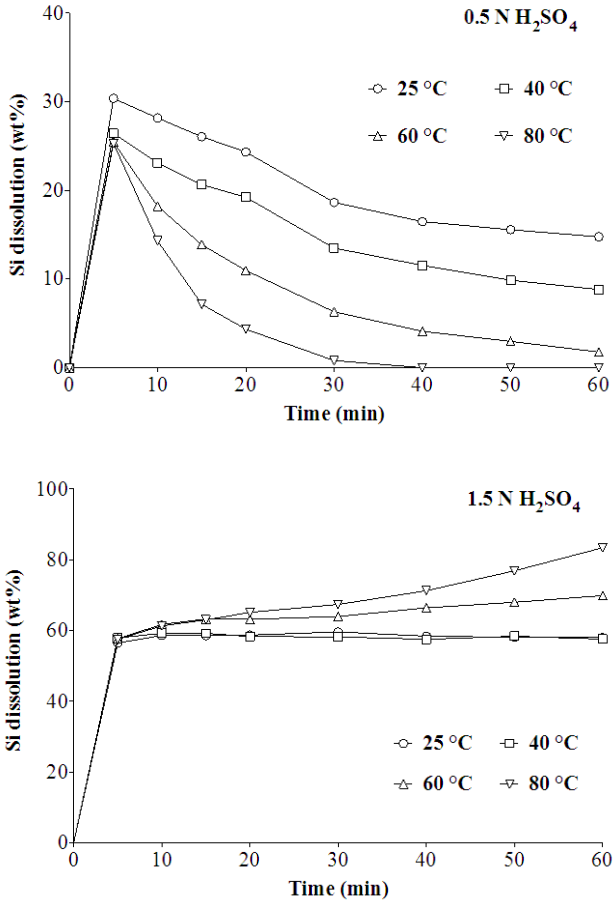

Figure 1. Effect of temperature on the dissolution of silicon during leaching of bauxite residue sample with different acid concentrations of H_2SO_4 (*L/S*: 5, 200 rpm).

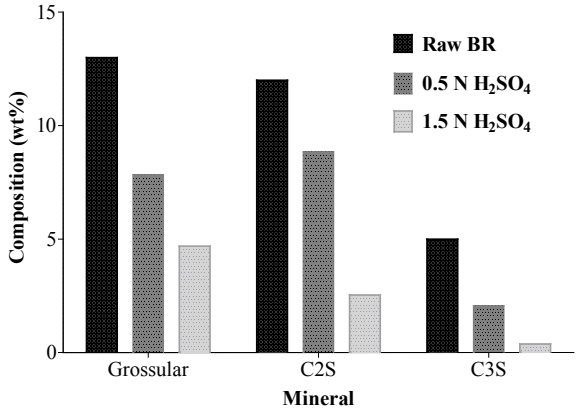

Figure 2. Concentration of selected mineralogical phases in the raw bauxite residue and in the solid after acidic leaching with H_2SO_4 (*T*: 80 °C, *L/S*: 5, *t*: 1 h).

Figure 3 describes the extraction behaviour of aluminium (Al), titanium (Ti) and iron (Fe) as function of silicon dissolution after acidic leaching of bauxite residue at different acid concentration and 80 °C. At low acid concentration, the extraction of Al, Fe or Ti was significantly low, because of an insufficient amount of acid devoted to leaching as the silicate compounds consumed part of the acid. However, an increase in the extraction of metal was observed at 1.5 N H_2SO_4 upon a significant amount of silicon dissolution.

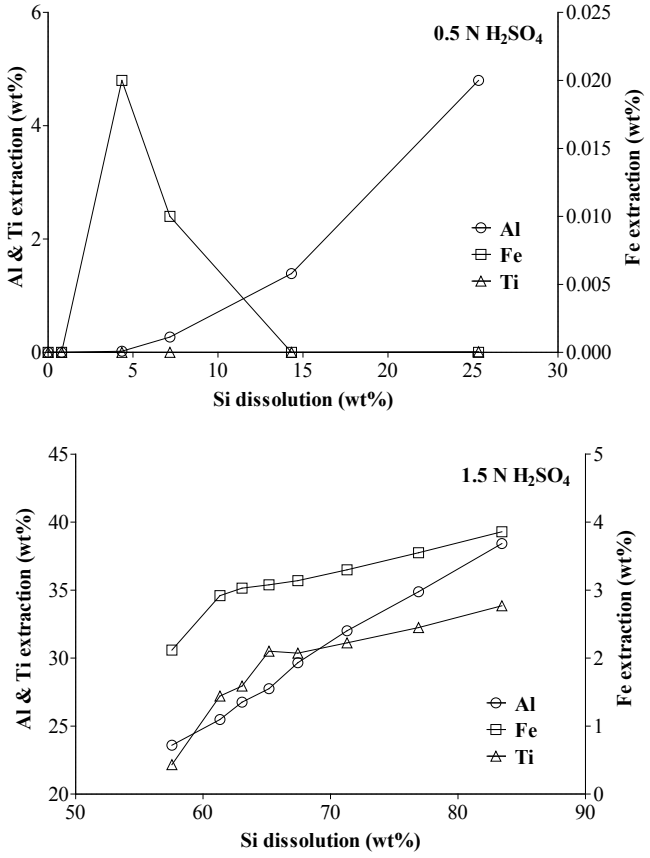

Figure 3. Extraction behaviour of Al, Ti and Fe as function of Si dissolution after acidic leaching of bauxite residue (*T*: 80 °C, *L/S*: 5, *t*: 1 h).

3.3. Reaction Mechanism for Silicon Dissolution

The reaction mechanisms were evaluated by considering the shrinking core model. The model was evaluated by diffusion control through production layer and first-order chemical control mechanism according to Equations 5 and 6, respectively,

$$1 - \frac{2}{3}\alpha - (1-\alpha)^{2/3} = k_d \cdot t \quad (5)$$

$$1 - (1-\alpha)^{1/3} = k_R \cdot t \quad (6)$$

where α represents the reacted (dissolved) fraction of silicon. The controlling mechanism was evaluated by plotting the algebraic function of reacted silicon $f(\alpha)$ versus time t. The correlation between the plotted data with a linear regression defines the controlling mechanism. k_d and k_R represent the rate constants for the diffusion and chemical reaction mechanism, respectively, and these rate constants may depend on diffusion rate, acid concentration, mineral density, particle size, equilibrium conditions and volume fraction of the particles [20]. On the basis of Equations 5 and 6, the apparent rate constant was calculated by the least square method at different temperatures (Table 3). The reaction mechanism at 0.5 N H_2SO_4 could not be established due to the precipitation of silicon. Figure 4 describes the reaction mechanism for silicon dissolution at 1.5 N H_2SO_4 and different temperatures.

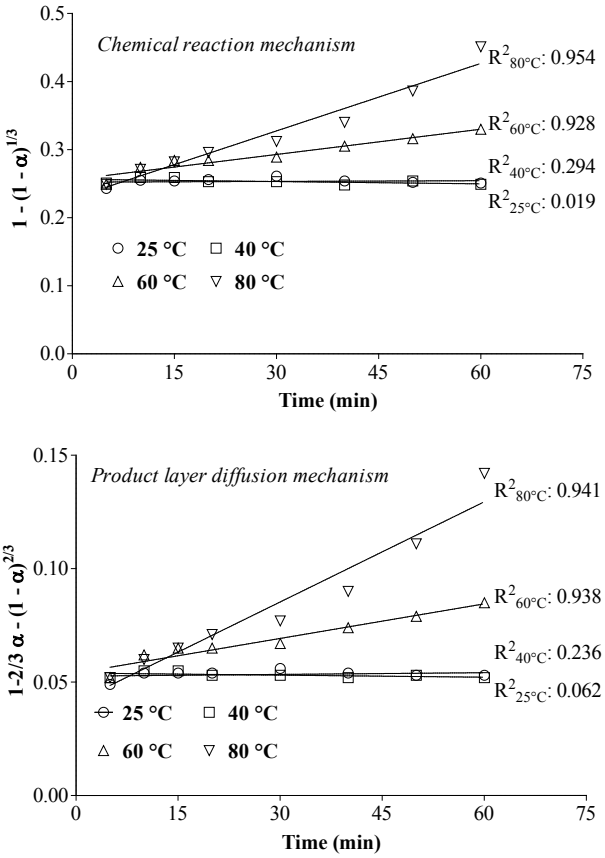

Figure 4. Reaction mechanism for silicon dissolution in the presence of 1.5 N H_2SO_4 at different temperatures. R-square (R^2) values are presented next to the corresponding regression line (*L/S*: 5, 200 rpm, *t*: 1 h).

The shrinking core model did not demonstrate a good correlation with experimental results at temperatures below 45 °C due to the slight decrease of silicon dissolution (Figure 1). At high

temperatures, i.e. above 55 °C, both mechanisms demonstrate a relatively good correlation with experimental data, i.e. $R^2 > 0.92$. This may indicate that the kinetic behavior at high temperatures is described by a two-stage model of first-order chemical reaction followed by diffusion stage. During the chemical reaction, silicon oxide on the surface of minerals is first leached out. The silicic acid formed during the acidic dissolution of silicate minerals transforms into silica gel product according to Equations 1 – 4. Therefore, the polymerization of silicic acid starts after the hydrolysis of silica [17] via condensation of monosilicic acid into cyclic oligomers [18] as it is represented by Equation 7:

$$H_3SiO_4^- + H_4SiO_4 \quad \leftrightarrows \quad (OH)_3Si\text{-}O\text{-}Si(OH)_3 + OH^- \qquad (7)$$

According to Equation 7, an oxygen atom bridges the silanol group, i.e. $Si(OH)_3$, in order to produce siloxane, i.e. Si – O – Si. The resultant oligomers polymerize by reacting with $H_3SiO_4^-$ until a gel network is formed via Ostwald ripening, i.e. dissolution of smaller particles and deposition on larger particles [7]. These deposits act as a resistance for the H_2SO_4 solution [19] and presumably be adsorbed on the surface of particles resulting in the leaching process being controlled by diffusion through this newly deposited layer. The rate controlling step at temperature above 55 °C was confirmed by the apparent activation energy (E_a) determined in accordance to the Arrhenius equation (Equation 8)

$$k = k_0 \cdot exp\left(-\frac{E_a}{RT}\right) \qquad (8)$$

where k represents the corresponding rate constant for the chemical reaction (k_R) and diffusion (k_d) mechanism. R is the ideal gas constant (kJ mol^{-1} K^{-1}) and T the temperature (K). k_0 defines a constant value for chemical reactions. The corresponding rate constants, k_d and k_R, were determined for both controlling mechanisms at different temperatures (Table 3). However, due to the non-reproducibility of experimental results at temperatures below 45 °C, only the rate constant at 60 and 80 °C were considered. Figure 5 describes the Arrhenius plot for product layer diffusion and chemical reaction mechanism. The activation energies are calculated from the slope of the corresponding line and are more than 40 kJ mol^{-1} but less than 90 kJ mol^{-1}, which confirms that the conversion rate is controlled by a mixing mechanism, i.e. material transport (product layer diffusion) and dissolved reaction products (chemical reaction) [20-21]. However, the above-mentioned models (Equations 5 and 6) cannot explain the reaction mechanism at low H_2SO_4 concentration and neither at low temperatures mainly due to precipitation of silica. It must be noticed that the shrinking core model considers a constant particle size, which in our study may not be the case due to the aggregation of silica monomers during acidic leaching [18]. It is believed that these aggregates may act as a resistance for the H_2SO_4 solution and partially adsorbed on the surface of bauxite residue minerals (Figure 6). This may result in the leaching process being controlled by diffusion through this newly deposited layer.

Table 3. Rate constants k_R and k_d with their correlation coefficients for silicon dissolution from bauxite residue at 1.5 N H_2SO_4.

Temperature	Apparent rate constants		Correlation coefficient	
	k_R (10^{-3} min^{-1})	k_d (10^{-3} min^{-1})	k_R	k_d
25	0.16	0.06	0.019	0.062
40	-0.04	51.59	0.294	0.236
60	1.47	0.60	0.928	0.938
80	3.68	1.65	0.954	0.941

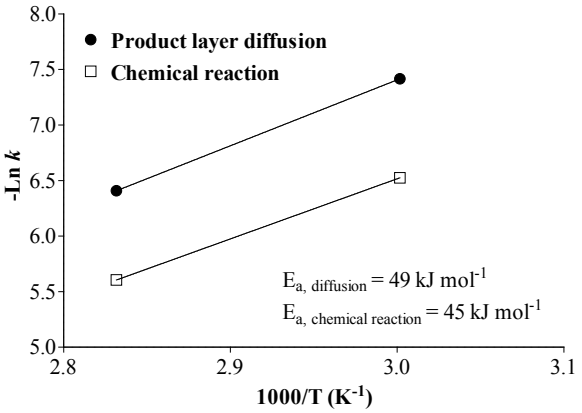

Figure 5. Arrhenius plot for product layer diffusion and chemical reaction mechanism (1.5 N H_2SO_4, *L/S*: 5, 200 rpm, *t*: 1 h).

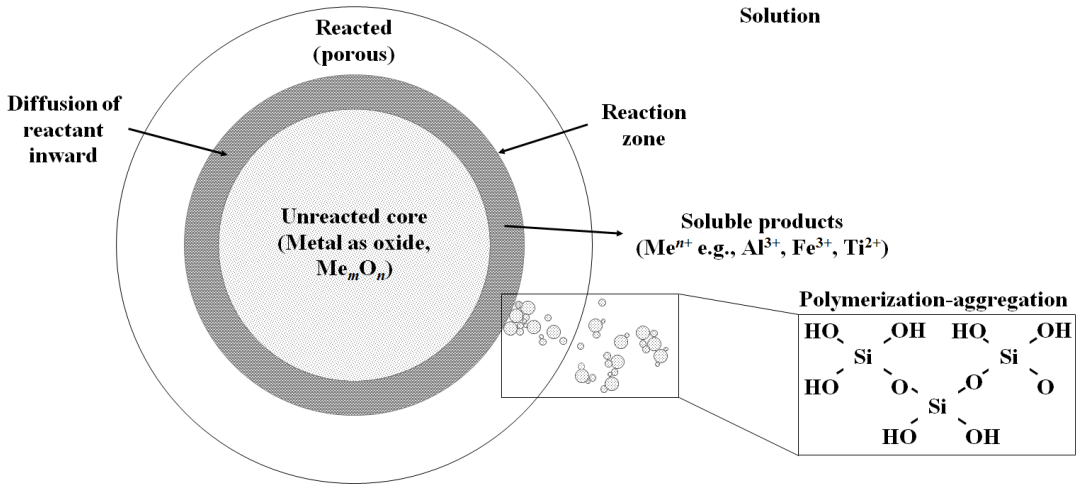

Figure 6. Illustration of metal leaching from a particle of bauxite residue with silica gel formation (i.e. silica polymerization and aggregation).

4 Conclusions

Kinetic studies demonstrated that, at constant temperatures, the dissolution of silicon in the leachate increases with increasing acid concentration, due to the high solubility in water of the orthosilicic acid at decreasing pH. However, the dissolution of silicon decreases when the temperature is increased, due to an increase of the silica saturation index. The hydrolysis of silica is the key stage to avoid silica polymerization during acidic leaching of bauxite residue.

The dissolution of silica from bauxite residue during acidic leaching is a very complex process controlled by a chemical reaction stage, i.e. silica gel formation as consequence of hydrolysis of silica, and a diffusion stage caused by the partial adsorption of this silica gel layer on the surface of the particles. However, the shrinking core model demonstrated limitations regarding the reproducibility of experimental data, because it does not consider aggregation of silica monomers formed during acidic leaching of bauxite residue.

5 Acknowledgements

The research leading to these results has received funding from the European Community's Horizon 2020 Programme (H2020/2014–2019) under Grant Agreement No. 636876 (MSCA-ETN REDMUD). This publication reflects only the author's view, exempting the Community from any liability. Project website: http://www.etn.redmud.org. The authors thank Aluminium of Greece for providing the bauxite residue sample.

6 References

1. Koen Binnemans et al., Towards zero-waste valorisation of rare-earth-containing industrial process residues: a critical review, *Journal of Cleaner Production*, Vol. 99, (2015), 17–38.
2. Chenna Rao Borra et al., Recovery of rare earths and other valuable metals from bauxite residue (red mud): a review, *J. Sustain. Metall*, Vol. 2, No. 4, (2016), 365–386.
3. Na Zhang, Hong-Xu Li, and Xiao-Ming Liu, Recovery of scandium from bauxite residue—red mud: a review, *Rare Metals*, Vol. 35, No. 12, (2016), 887–900.
4. Weiwei Wang, Yoko Pranolo, and Chu Yong Cheng, Metallurgical processes for scandium recovery from various resources: A review, *Hydrometallurgy*, Vol. 108, No. 1–2, (2011), 100–108.
5. Zhaobo Liu and Hongxu Li, Metallurgical process for valuable elements recovery from red mud—A review, *Hydrometallurgy*, Vol. 155, (2015), 29–43.
6. P. Kokhanenko, K. Brown, and M. Jermy, Silica aquasols of incipient instability: Synthesis, growth kinetics and long term stability, *Colloids and Surfaces A: Physicochem. Eng. Aspects*, Vol. 493, (2016), 18–31.
7. Dominique J. Tobler, Sam Shaw, and Liane G. Benning, Quantification of initial steps of nucleation and growth of silica nanoparticles: An in-situ SAXS and DLS study, *Geochimica et Cosmochimica Acta*, Vol. 73, No. 18, (2009), 5377–5393.
8. Aly A. Hamouda and Hossien A. Akhlaghi Amiri, Factors affecting alkaline sodium silicate gelation for in-depth reservoir profile modification, *Energies*, Vol. 7, No. 2, (2014), 568–590.
9. Jan Schlomach and Matthias Kind, Investigations on the semi-batch precipitation of silica, *Journal of Colloid and Interface Science*, Vol. 277, No. 2, (2004), 316–326.
10. Sebastian Wilhelm and Matthias Kind, Influence of pH, temperature and sample size on natural and enforced syneresis of precipitated silica, *Polymers*, Vol. 7, No. 12, (2015), 2504–2521.
11. D. Voßenkaul et al., Hydrometallurgical processing of eudialyte bearing concentrates to recover rare earth elements via low-temperature dry digestion to prevent the silica gel formation, *Journal of Sustainable Metallurgy*, Vol. 3, No. 1, (2017), 79–89.
12. Yadong Zhang et al., Recovery of zinc from a low-grade zinc oxide ore with high silicon by sulfuric acid curing and water leaching, *Hydrometallurgy*, Vol. 166, (2016), 16–21.
13. E. Abkhoshk et al., Review of the hydrometallurgical processing of non-sulfide zinc ores, *Hydrometallurgy*, Vol. 149, (2014), 153–167.
14. Lina Shi et al., Desilication of low alumina to caustic liquor seeded with sodalite or cancrinite, *Hydrometallurgy*, Vol. 170, (2017), 5-15.
15. T.W. Zerda, I. Artaki, and J. Jonas, Study of polymerization processes in acid and base

catalyzed silica sol-gels, *Journal of Non-Crystalline Solids*, Vol. 81, No. 3, (1986), 365–379.

16. Mary W. Colby, A. Osaka, and J.D. Mackenzie, Effects of Temperature on Formation of Silica Gel, *Journal of Non-Crystalline Solids*, Vol. 82, (1986), 37–41.
17. C.A. Milea, C. Bogatu, and A. Duta, The Influence of Parameters in Silica Sol-Gel Process, *Bulletin of Transilvania University of Brasov: Engineering Sciences*, Vol. 4, No. 1, (2011), 59–66.
18. Elizabeth A. Gorrepati et al., Silica precipitation in acidic solutions: Mechanism, pH effect, and salt effect, *Langmuir*, Vol. 26, No. 13, (2010), 10467–10474.
19. Fuqiang Zheng et al., Kinetics of Hydrochloric Acid Leaching of Titanium from Titanium-Bearing Electric Furnace Slag, *JOM*, Vol. 68, No. 5, (2016), 1476–1484.
20. Fathi Habashi, Principles of Extractive Metallurgy, General Principles, 2nd ed. (New York: Gordon and Breach Science Publishers, Inc.), 1969, pp. 111–169.
21. Hong Y. Sohn, Milton E. Wadsworth, Rate Processes of Extractive Metallurgy (New York: Plenum Press), 1979, pp. 135– 143.